Original Article

Integrated bioinformatics and machine learning algorithms reveal the unfolded protein response pathways and immune infiltration in acute myocardial infarction

Yang Bai[1], Zequn Niu[2], Zhenyu Yang[3], Yi Sun[1], Weidong Yan[1], Anshi Wu[1], Changwei Wei[1]

[1]Department of Anesthesiology, Beijing Chao-Yang Hospital, Capital Medical University, Beijing, China; [2]Computer Science and Technology, The Open University of China, Beijing, China; [3]Department of Endocrinology, South China Hospital of Shenzhen University, Shenzhen, China

Contributions: (I) Conception and design: Y Bai, C Wei; (II) Administrative support: C Wei; (III) Provision of study materials or patients: Y Bai, Y Sun, W Yan; (IV) Collection and assembly of data: Y Bai, Z Yang; (V) Data analysis and interpretation: Y Bai, Z Niu; (VI) Manuscript writing: All authors; (VII) Final approval of manuscript: All authors.

Correspondence to: Changwei Wei, PhD. Department of Anesthesiology, Beijing Chao-Yang Hospital, Capital Medical University, 8 Gongren Tiyuchang Nanlu, Chaoyang District, Beijing 100020, China. Email: changwei.wei@ccmu.edu.cn.

Background: The unfolded protein response (UPR) is a critical biological process related to a variety of physiological functions and cardiac disease. However, the role of UPR-related genes in acute myocardial infarction (AMI) has not been well characterized. Therefore, this study aims to elucidate the mechanism and role of the UPR in the context of AMI.

Methods: Gene expression profiles related to AMI and UPR pathway were downloaded from the Gene Expression Omnibus database and PathCards database, respectively. Differentially expressed genes (DEGs) were identified and then functionally annotated. The random forest (RF) and least absolute shrinkage and selection operator (LASSO) regression analysis were conducted to identify potential diagnostic UPR-AMI biomarkers. Furthermore, the results were validated by using external data sets, and discriminability was measured by the area under the curve (AUC). A nomogram based on the feature genes was developed to predict the AMI-risk rate. Then we utilized two algorithms, CIBERSORT and MCPcounter, to investigate the relationship between the key genes and immune microenvironment. Additionally, we performed uniform clustering of AMI samples based on the expression of UPR pathway-related genes. The weighted gene co-expression network analysis was conducted to identify the key modules in various clusters, enrichment analysis was performed for the genes existing in different modules.

Results: A total of 14 DEGs related to the UPR pathway were identified. Among the 14 DEGs, *CEBPB*, *ATF3*, *EIF2S3*, and *TSPYL2* were subsequently identified as biomarkers by the LASSO and RF algorithms. A diagnostic model was constructed with these four genes, and the AUC was 0.939. The calibration curves, receiver operating characteristic (ROC) curves, and the decision curve analysis of the nomogram exhibited good performance. Furthermore, immune cell infiltration analysis revealed that four feature genes were linked with the infiltration of immune cells such as neutrophils. The cluster analysis of the AMI samples identified two distinct clusters, each with differential expression of genes related to the UPR pathway, immune cell infiltration, and inflammatory cytokine secretion. Weighted gene coexpression network analysis and enrichment analysis showed that both clusters were associated with the UPR.

Conclusions: Our study highlights the importance of the UPR pathway in the pathogenesis of myocardial infarction, and identifies four genes *CEBPB*, *ATF3*, *EIF2S3*, and *TSPYL2* as diagnostic biomarkers for AMI, providing new ideas for the clinical diagnosis and treatment of AMI.

Keywords: Unfolded protein response (UPR); acute myocardial infarction (AMI); bioinformatics; immune cell infiltration; weighted gene coexpression network analysis (WGCNA)

Submitted Apr 14, 2024. Accepted for publication Aug 30, 2024. Published online Oct 30, 2024.
doi: 10.21037/jtd-24-622
View this article at: https://dx.doi.org/10.21037/jtd-24-622

Introduction

Acute myocardial infarction (AMI) is caused by coronary artery occlusion, resulting in localized heart tissue ischaemia, hypoxia and necrosis, and is one of the leading causes of mortality worldwide (1). It is estimated that annually, more than 7 million individuals succumb to this disease, and this number is expected to increase to more than 9 million by 2030 (2). Clinical management of AMI aims to restore blood flow, and the main treatment methods include pharmacologic thrombolysis, vascular intervention or coronary angioplasty (3). Considerable improvements in the approaches for the prevention and treatment of AMI have occurred in recent decades. However, the incidence of myocardial infarction (MI) has not declined; in fact, it has increased (4). Early and accurate diagnosis of AMI is an important step to reduce the incidence of adverse events and improve the survival rate of AMI patients, especially for patients with atypical symptoms. Exploring the signalling pathways underlying the pathogenesis of MI has great potential for improving diagnosis and treatment.

The mitochondrial unfolded protein response (UPR) is considered the first line of defence against mitochondrial damage triggered by the accumulation of misfolded proteins within mitochondria (1). The mitochondrial UPR promotes the expression of mitochondrial protective genes encoded by nuclear DNA and mitochondrial DNA, and initiates the transcriptional activation program of mitochondrial chaperones and proteases to alleviate the abnormal protein accumulation within the mitochondria, thereby restoring mitochondrial protein homeostasis and protecting cells from extensive mitochondrial stress (1,5). When mitochondrial stress exceeds a certain threshold, the UPR is unable to fully repair the damaged mitochondria, triggering mitophagy to remove the dysfunctional mitochondria (6). The mechanisms regulating the mitochondrial UPR are complex. A recent study has shown that endoplasmic reticulum stress, mitophagy, inflammation, hypoxia, apoptosis and mitochondrial dysfunction are closely related to UPR (5). Aberrant UPR contributes to various diseases such as diabetes, cancers and obesity (7). Given the pleiotropic effects of UPR, in-depth research on UPR pathway-related genes in AMI will further enhance our understanding of the pathological mechanisms of AMI and find potential therapeutic approaches for AMI.

The development of bioinformatics analysis techniques has provided us with the ability to research the detailed regulatory mechanisms of complex disease occurrence and development (8). As a core field of artificial intelligence, machine learning has been widely used in the medical field. Machine learning can identify key biomarkers for the diagnosis and prognosis of diseases and has shown great potential in medical fields such as biomedical research and personalized medicine (9). In the present study, we downloaded the human AMI transcriptome dataset and UPR pathway-related genes from the Gene Expression Omnibus (GEO) database and PathCards database, respectively. The power of bioinformatics and two machine learning algorithms, random forest (RF) and least absolute shrinkage and selection operator (LASSO), were leveraged to identify key biomarkers related to the UPR pathway and gain new insights into the potential mechanisms underlying AMI. We hope this research will provide a foundation for the diagnosis and treatment of AMI and reduce the burden of this disease. We present this article in accordance with the TRIPOD reporting checklist (available at https://jtd.amegroups.com/article/view/10.21037/jtd-24-622/rc).

Highlight box

Key findings

- We identified four genes *CEBPB*, *ATF3*, *EIF2S3*, and *TSPYL2* as diagnostic biomarkers for acute myocardial infarction (AMI). A diagnostic model was constructed with these four genes, and the area under the curve was 0.939.

What is known and what is new?

- Unfolded protein response (UPR) is a critical biological process related to a variety of physiological functions and cardiac disease.
- The role of UPR-related genes in AMI has not been well characterized. The present study identified *CEBPB*, *ATF3*, *EIF2S3*, and *TSPYL2* as the critical UPR genes for AMI.

What is the implication, and what should change now?

- *CEBPB*, *ATF3*, *EIF2S3*, and *TSPYL2* may be potential therapeutic targets for AMI. We constructed a nomogram that can help clinicians identify high-risk individuals, and thus help guide treatment decisions for myocardial infarction patients.

Methods

Data download

The study was conducted in accordance with the Declaration of Helsinki (as revised in 2013). Microarray expression data, including the GSE66360 and GSE14975 datasets, were downloaded from the GEO database. GPL570 (HG-U133_Plus_2; Affymetrix Human Genome U133 Plus 2.0 Array) served as the detection platform for both databases. The GSE66360 dataset was divided into a training set (21 AMI patients and 22 healthy control individuals) and a validation set (28 AMI patients and 28 healthy control individuals). The GSE14975 dataset was used as the reverse validation set [5 atrial fibrillation (AF) patients and 5 healthy control individuals]. All the datasets were subjected to standardized data preprocessing. The UPR pathway-related genes were downloaded from the PathCards database.

Analysis of differentially expressed genes (DEGs) related to the UPR pathway

Differential expression analysis of mRNA data was conducted using the "limma" package (version 4.3.1), setting the criteria of a $|\log_2[\text{fold change (FC)}]| > 0.2$ and P value <0.05 (10). The "ComplexHeatmap" package was used to generate heatmaps to reveal the expression patterns of these genes. We also analysed the correlations among DEGs and generated correlation heatmaps with the "ggplot2" package. In addition, we used the "GSVA" package to assess the single sample gene set enrichment analysis (ssGSEA) scores of the UPR pathway genes in the AMI and control groups. These results provide a foundation for exploring the role of the UPR pathway in AMI patients.

Functional enrichment analyses

Gene Ontology (GO) analysis, which includes molecular function (MF), biological process (BP) and cellular component (CC) ontologies, was used to describe the properties of genes and gene products. Kyoto Encyclopedia of Genes and Genomes (KEGG) enrichment analysis was used to identify pathways associated with the DEGs. We performed GO and KEGG analyses with the "clusterProfiler" (version 4.4.4) package. The results of the enrichment analysis were visualized with the "ggplot2" package (11).

Single-gene GSEA enrichment analysis is implemented in the "GSEA" package in R. And we utilized the GO pathway set as the background gene set to perform GSEA analysis on each marker gene.

Screening key genes by machine learning and model building

Two distinct algorithms (LASSO and RF) were utilized to select key genes associated with the UPR pathway. The "glmnet" and "randomForest" packages were utilized for LASSO and RF analysis, respectively. The LASSO algorithm is a linear regression method that shrinks regression coefficients and sets some unimportant coefficients to shrink to zero (12). The RF algorithm was used to estimate the importance of each gene (13). We listed the seven genes with the highest values for MeanDecreaseGini, a RF prediction metric. Furthermore, key biomarkers for AMI were identified by overlapping genes derived from the two machine learning algorithms. Next, we assessed the predictive value of key biomarkers by quantifying their sensitivity and specificity using the "pROC" package and measuring the area under the receiver operating characteristic (ROC) curve (14). The area under the curve (AUC) was calculated as the predicted value of the key biomarkers in the training set and further validated in the validation and reverse validation set (GSE14975). Subsequently, the key genes were analysed by multivariable logistic regression, and a nomogram was generated using the "regplot" package to depict the key gene columns. Additionally, we performed decision curve analysis (DCA) to estimate the utility of the models for decision making and generated calibration curves to assess the performance and internal validity of the nomogram. The decision curves and clinical calibration curves were plotted using the "rmda" and "rms" packages, respectively. Moreover, the Hosmer-Lemeshow test was used to assess the goodness of fit of the multivariable model, and a Hosmer-Lemeshow statistic >0.05 indicated good calibration. A correlation diagram of key genes was generated using the "ggstatsplot" package.

Immune infiltration analysis

Two cutting-edge algorithms, the CIBERSORT algorithm and the MCPcounter algorithm, were both used to calculate the relationships between the key genes and immune cells (15,16). Bar graphs were drawn to show the differential expression levels of immune infiltrating cells in the AMI group and control group. Pearson correlation analysis was

performed to determine the correlations between the hub genes and infiltrating immune cells, and the results were visualized using the 'ggcorrplot' package.

Consensus clustering analysis

We used the R package "ConsensusClusterPlus" to perform cluster analysis on the genes related to the UPR pathway in AMI patients (17). In the consensus clustering matrix at k=2, the samples are clearly clustered into two clusters. Then, the "ComplexHeatmap" package was used to construct a heatmap of gene expression in two clusters of AMI patients. In addition, we used the "GSVA" package to assess the ssGSEA scores of the UPR pathway genes in different clusters, and the results were visualized through a violin plot. The relationships between distinct clusters and immune cells and inflammatory factor expression were visualized through bar graphs.

Enrichment analysis of different clusters

We utilized the "weighted gene coexpression network analysis (WGCNA)" package to analyse the gene expression matrix of the distinct clusters (18). The "goodSampleGenes" function was used to check the integrity of the data. The ideal soft threshold (R^2=0.9, β=4) was calculated by the "pickSoftThreshold" algorithm to construct a scale-free network. Then, we transformed the matrix data into an adjacency matrix to cluster gene modules with a dynamic tree-cutting algorithm, and the minimum size of the modules was 30 genes. In addition, we visualized the correlations between different clusters and gene modules using the "labeledHeatmap" function. The "anRichment" package was used to conduct an enrichment analysis of the gene module clusters.

Statistical analysis

All analyses were performed with R statistical software (version 4.3.1). When constant variables between groups were normally distributed, an unpaired Student's *t*-test was used. When constant variables were not normally distributed, the Mann-Whitney *U* test was used. Pearson correlation analysis was used to reveal the relationships between genes and infiltrating immune cells. A P value less than 0.05 indicated statistical significance.

Results

Expression of UPR pathway-related genes in AMI patients

In this study, a total of 89 genes related to the UPR pathway were identified in the training set, and the clustering heatmap showed the expression patterns of UPR-related genes among the samples (*Figure 1A*). Fourteen of the 89 UPR pathway-related genes were significantly differentially expressed. Correlation analysis revealed a high degree of correlation among these genes (*Figure 1B*). These findings indicate that a single change in gene expression in the UPR pathway often results in a cascading reaction involving multiple genes. Furthermore, the ssGSEA score of the AMI group was significantly greater than that of the control group, indicating a significant increase in UPR pathway activation in AMI patients (*Figure 1C*).

Functional analysis of the UPR-related DEGs

GO enrichment revealed that the UPR-related DEGs were significantly related to the functions "response to endoplasmic reticulum stress", "response to topologically incorrect protein", and "response to unfolded protein" in the BP category. They were related to "transcription regulator complex" and "RNA polymerase II transcription regulator complex" in the CC category. In the MF category, they were related to "DNA-binding transcription activator activity", "DNA-binding transcription activator activity, RNA polymerase II-specific", and "protein heterodimerization activity". KEGG analysis indicated that the "lipid and atherosclerosis" and "protein processing in endoplasmic reticulum" pathways were enriched (*Figure 2*).

Four UPR-related DEGs as diagnostic genes for AMI

Next, we utilized two distinct algorithms, LASSO and RF, to screen the feature genes from the training set. For the LASSO algorithm, following 10-fold cross-validation, a set of 8 genes, namely, *CEBPB*, *ATF3*, *DNAJC3*, *EIF2S3*, *DNAJB11*, *EXOSC3*, *TSPYL2*, and *CCL2*, was selected (*Figure 3A,3B*). For the RF algorithm, we screened 7 genes with the highest values for MeanDecreaseGini, namely, *CEBPB*, *DDIT3*, *ATF3*, *EIF2S3*, *TSPYL2*, *DNAJB11*, and *CXCL8* (*Figure 3C*). Finally, 5 key genes (*CEBPB*, *ATF3*, *EIF2S3*, *TSPYL2*, and *DNAJB11*) shared between the LASSO and RF algorithms were identified as diagnostic

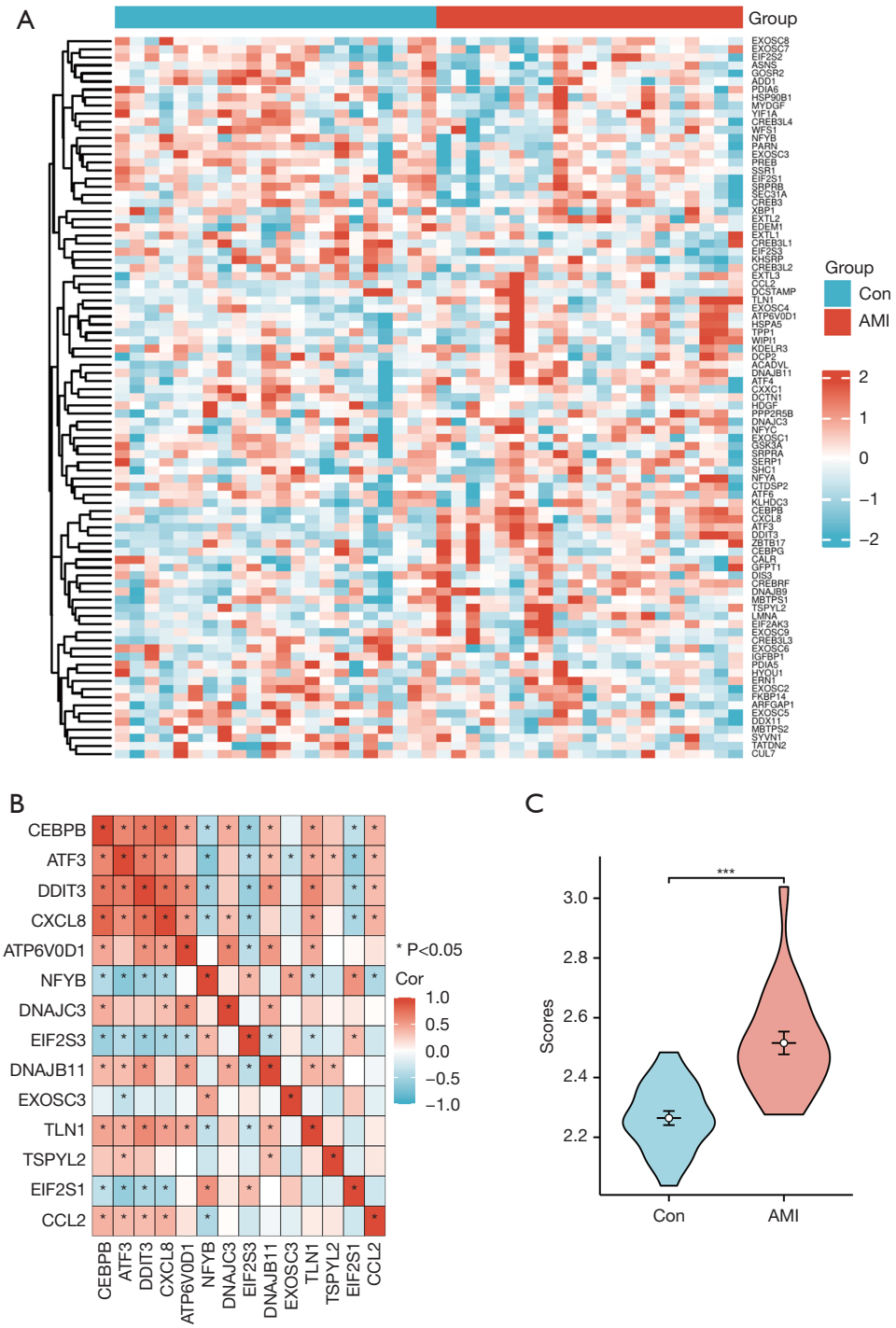

Figure 1 UPR pathway-related genes in AMI patients. (A) Heatmap of UPR pathway-related genes. (B) The correlation of differential gene in the UPR pathway. (C) Violin plots show the difference of ssGSEA scores between the two groups. *, P<0.05; ***, P<0.001. AMI, acute myocardial infarction; Con, control; Cor, correlation; UPR, unfolded protein response; ssGSEA, single sample gene set enrichment analysis.

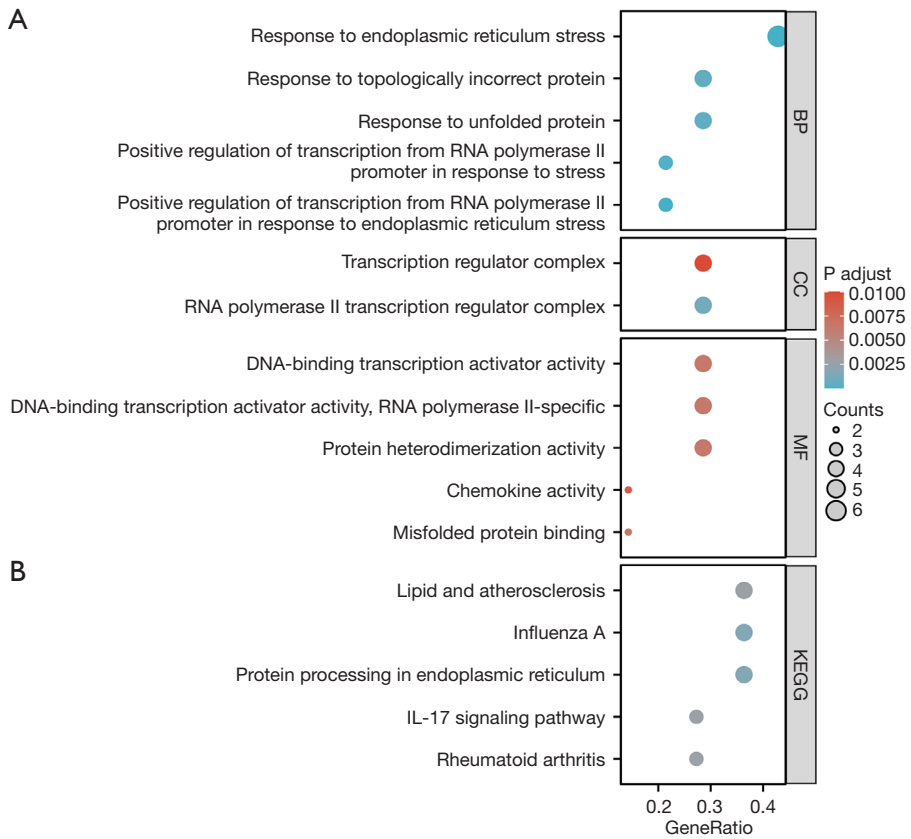

Figure 2 Functional enrichment analysis. (A) The partial terms of the GO pathways. (B) The partial terms of the KEGG pathways. GO, Gene Ontology; BP, biological progress; CC, cellular component; MF, molecular function; KEGG, Kyoto Encyclopedia of Genes and Genomes.

markers for further analysis (*Figure 3D*). Notably, the AUC values of the 5 key genes were greater than 0.75, indicating that these 5 genes might serve as diagnostic markers for AMI patients (*Figure 3E*).

In addition, we further verified the reliability and reproducibility of the 5 diagnostic genes in the validation set. The results showed that *CEBPB*, *ATF3*, *EIF2S3*, and *TSPYL2* were differentially expressed between the AMI group and the control group (*Figure 3F*). Then, the discriminatory ability of the nomogram was confirmed by ROC analysis. As shown in *Figure 4A*, the AUC of *CEBPB* was 0.728, the AUC of *ATF3* was 0.898, the AUC of *EIF2S3* was 0.74, and the AUC of *TSPYL2* was 0.718. The diagnostic model constructed from these four genes (*CEBPB* + *ATF3* + *EIF2S3* + *TSPYL2*) showed excellent performance, with an AUC of 0.939, which was greater than that of the individual genes. However, in the AF dataset GSE14975, the expression of *CEBPB*, *ATF3*, *EIF2S3* and *TSPYL2* did not significantly differ (*Figure 4B*). Based on these results, the biomarkers *CEBPB*, *ATF3*, *EIF2S3* and *TSPYL2* have high diagnostic accuracy. A nomogram model was constructed with four diagnostic markers (*CEBPB*, *ATF3*, *EIF2S3* and *TSPYL2*), and *CEBPB* and *ATF3* had the greatest diagnostic significance for AMI patients (*Figure 4C*). Then, we used clinical calibration and DCA to evaluate the clinical effect of the nomogram model (*Figure 4D*). The DCA results showed that the *CEBPB* + *ATF3* + *EIF2S3* + *TSPYL2* curve was significantly greater than the grey curve, indicating the high accuracy of the nomogram model. In addition, a calibration curve was constructed to assess the predictive ability of the nomogram model. According to the calibration curve, the actual risk of AMI was close to the predicted risk, and a Hosmer-Lemeshow P value >0.05 indicated a high degree of accuracy in predicting AMI (*Figure 4E*). In addition, our analysis also revealed a strong positive correlation between

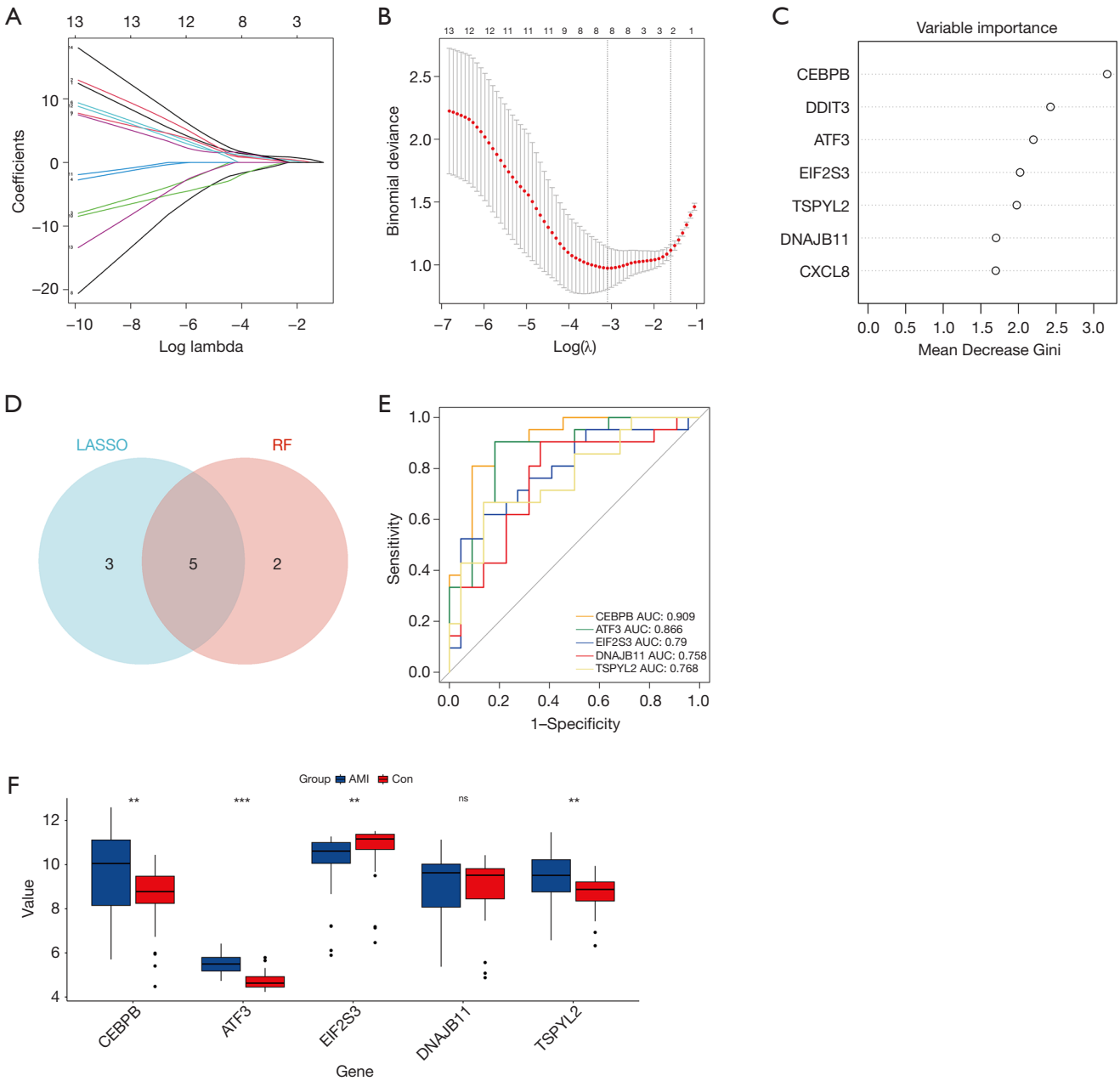

Figure 3 Screening of key genes. (A) LASSO coefficient profiles of UPR-related differential genes. (B) Cross-validation to select the optimal tuning parameter log Lambda in LASSO regression analysis. (C) RF analysis. (D) The key genes extracted from the LASSO and RF algorithms. (E) ROC curve of key genes in the training set. (F) Validation of the expression of the key genes by boxplot in the validation set. **, P<0.01; ***, P<0.001. ns, not significant; AMI, acute myocardial infarction; Con, control; LASSO, least absolute shrinkage and selection operator; UPR, unfolded protein response; RF, random forest; ROC, receiver operating characteristic.

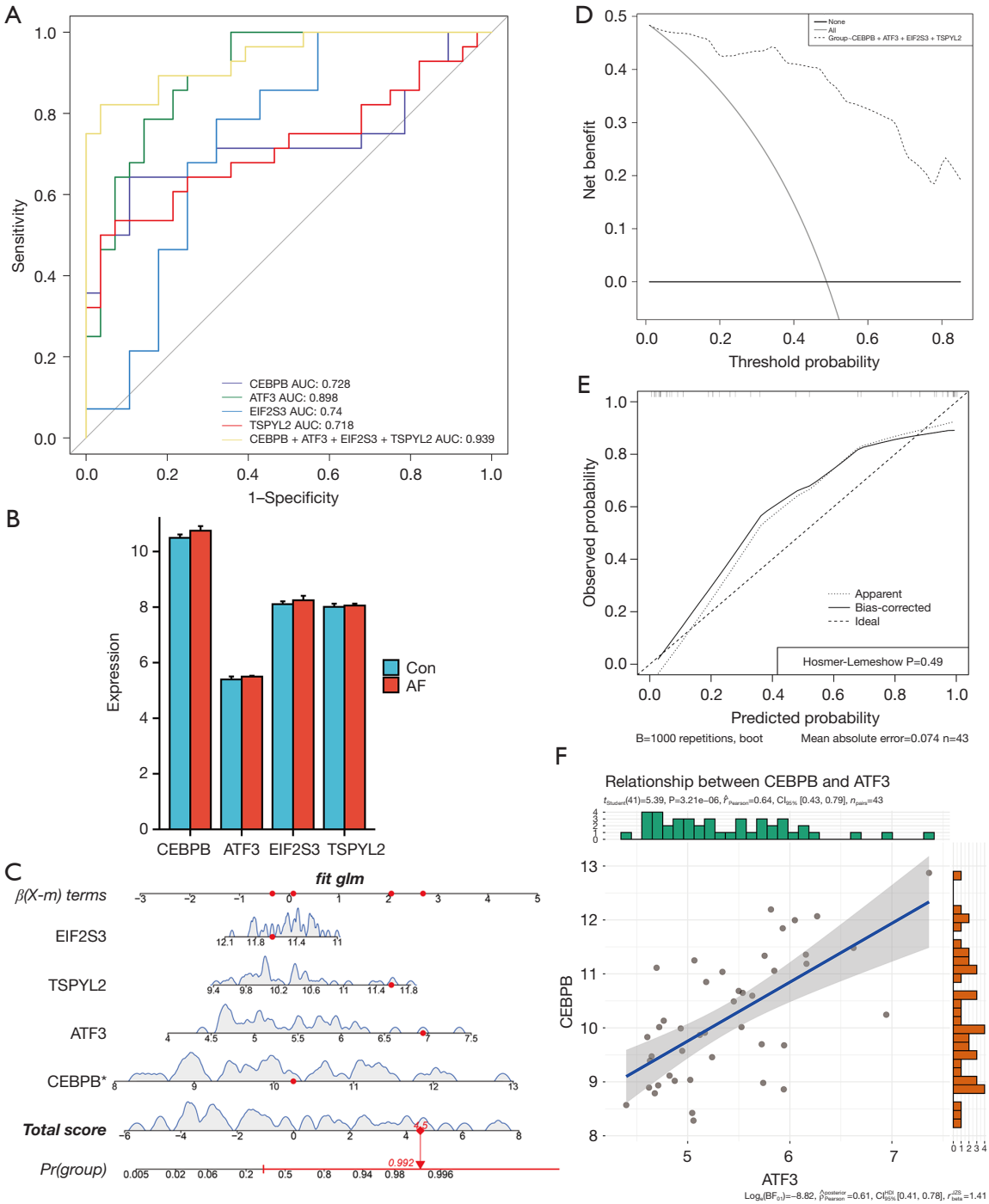

Figure 4 Key biomarkers validation and model construction. (A) ROC curve of the key biomarkers in the validation set. (B) Validation of the expression of key biomarkers in the reverse validation set (GSE14975). (C) Nomogram plot. (D) DCA clinical decision curve. (E) Clinical calibration curve. (F) Correlation plot between *ATF3* and *CEBPB*. *, P<0.05. Con, control; AF, atrial fibrillation; ROC, receiver operating characteristic; DCA, decision curve analysis.

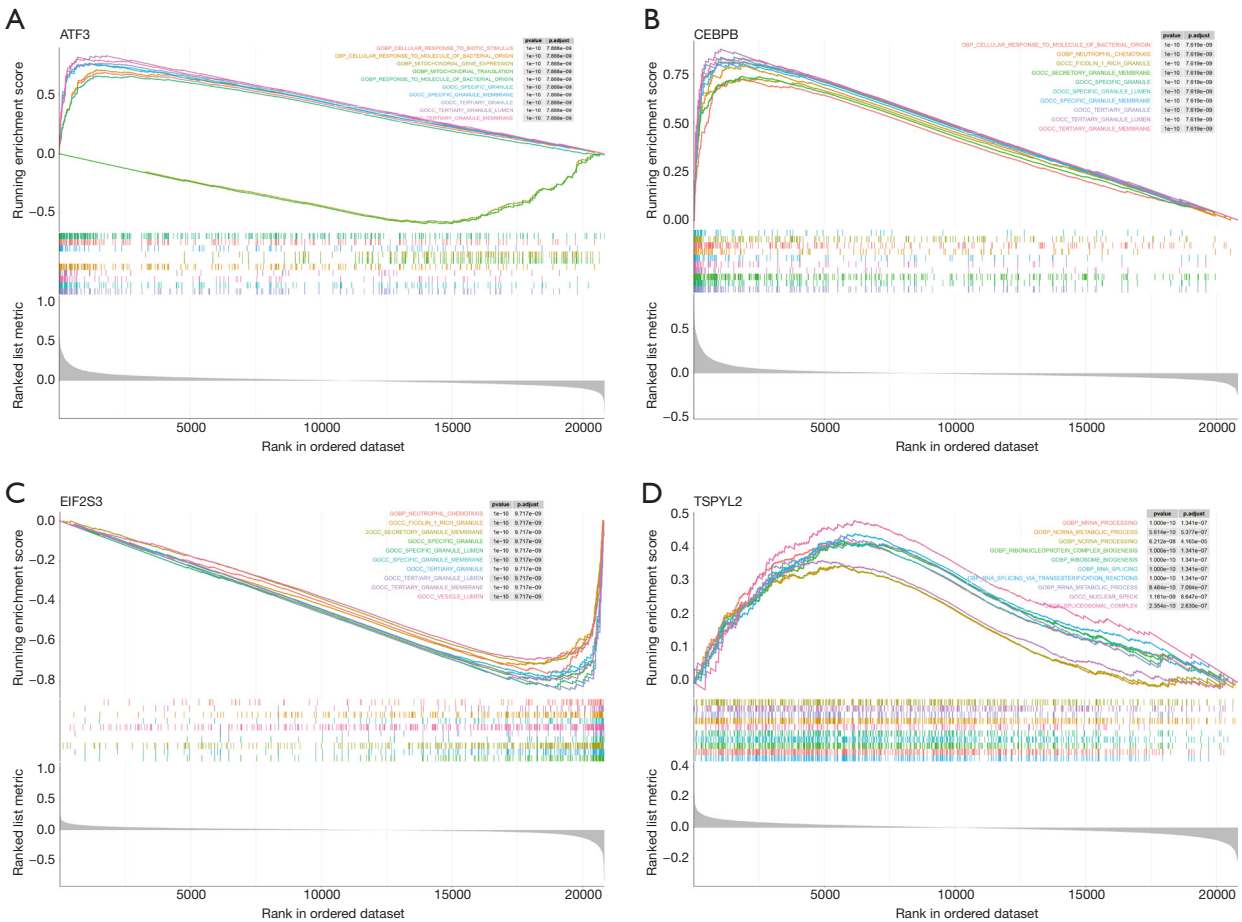

Figure 5 Single-gene GO-GSEA pathway analysis in *ATF3* (A), *CEBPB* (B), *EIF2S3* (C), *TSPYL2* (D). GO, Gene Ontology; GSEA, gene set enrichment analysis.

CEBPB and *ATF3*, indicating that these two genes may have synergistic effects on AMI patients (*Figure 4F*).

Pathway analysis of the feature biomarkers

To further explore the potential functions of marker genes, we performed a single-gene GO-GSEA pathway analysis. The top 10 pathways enriched for each marker gene were illustrated in *Figure 5A-5D*. Candidate diagnostic genes were mainly enriched in the mitochondrial gene expression, mitochondrial translation, specific granule, tertiary granule, neutrophil chemotaxis, ficolin 1 rich granule, vesicle lumen, mRNA processing and ribonucleoprotein complex biogenesis. We propose that *CEBPB*, *ATF3*, *EIF2S3*, *TSPYL2* are not only related to mitochondrial UPR but may also be associated with immune response.

Immune infiltration analysis based on marker genes

We used both the CIBERSORT and MCPcounter algorithms to determine the associations between the four marker genes and the immune microenvironment in AMI patients. According to the CIBERSORT algorithm, the proportions of resting $CD4^+$ memory T cells and gamma delta T cells in AMI patients were lower than those in control individuals, and activated memory $CD4^+$ T cells, resting natural killer (NK) cells, monocytes, activated dendritic cells, activated mast cells and neutrophils were more highly expressed in AMI patients (*Figure 6A*). In addition, Pearson correlation analysis revealed that *CEBPB* was strongly positively correlated with eosinophils, activated mast cells, activated monocytes and neutrophils, activated resting NK cells, activated memory $CD4^+$ T cells, and

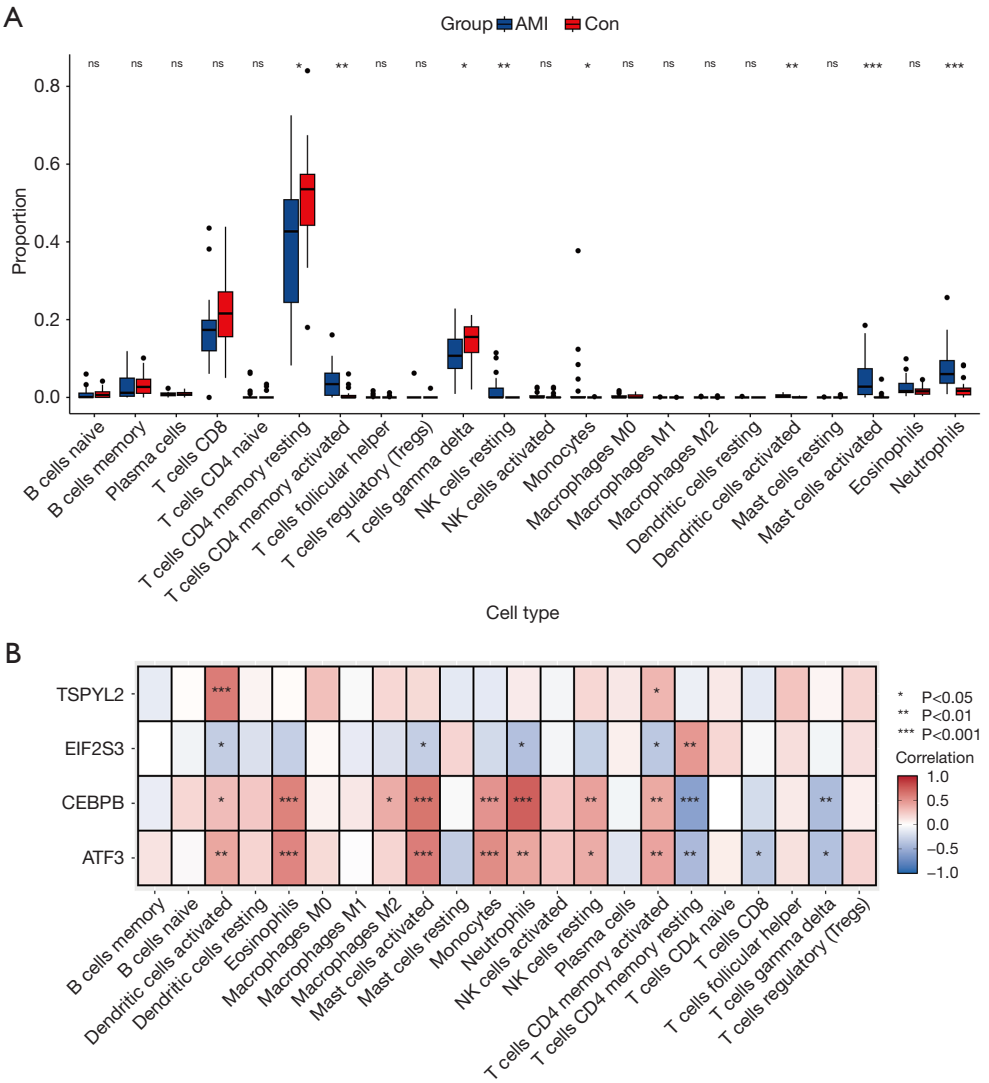

Figure 6 Immune landscape analysis by CIBERSORT algorithm. (A) Using the CIBERSORT algorithm to explore the differences in the immune microenvironment between AMI patients and normal controls. (B) Using the CIBERSORT algorithm to analysis immune cell infiltration of model genes. *, P<0.05; **, P<0.01; ***, P<0.001. ns, not significant; AMI, acute myocardial infarction; Con, control; NK, natural killer.

negatively correlated with resting memory CD4⁺ T cells and gamma delta T cells. *ATF3* was positively correlated with activated dendritic cells, activated eosinophils, activated mast cells, monocytes, activated neutrophils and activated memory CD4⁺ T cells but negatively correlated with resting memory CD4⁺ T cells. *TSPYL2* and *EIF2S3* were strongly positively correlated with activated dendritic cells and resting memory CD4⁺ T cells (*Figure 6B*). Further analysis using MCP-counter showed that the proportions of monocytes, neutrophils and endothelial cells in AMI patients were greater than those in control individuals (*Figure 7A*). Pearson correlation analysis revealed that *CEBPB* was positively correlated with endothelial cells, monocytic lineage cells, myeloid dendritic cells and neutrophils but negatively correlated with T cells. *ATF3* was positively correlated with endothelial cells, fibroblasts, monocytic lineage cells, myeloid dendritic cells and neutrophils but negatively correlated with T cells. *EIF2S3* expression was negatively correlated with the number of endothelial cells, monocytic lineage cells, and neutrophils (*Figure 7B*).

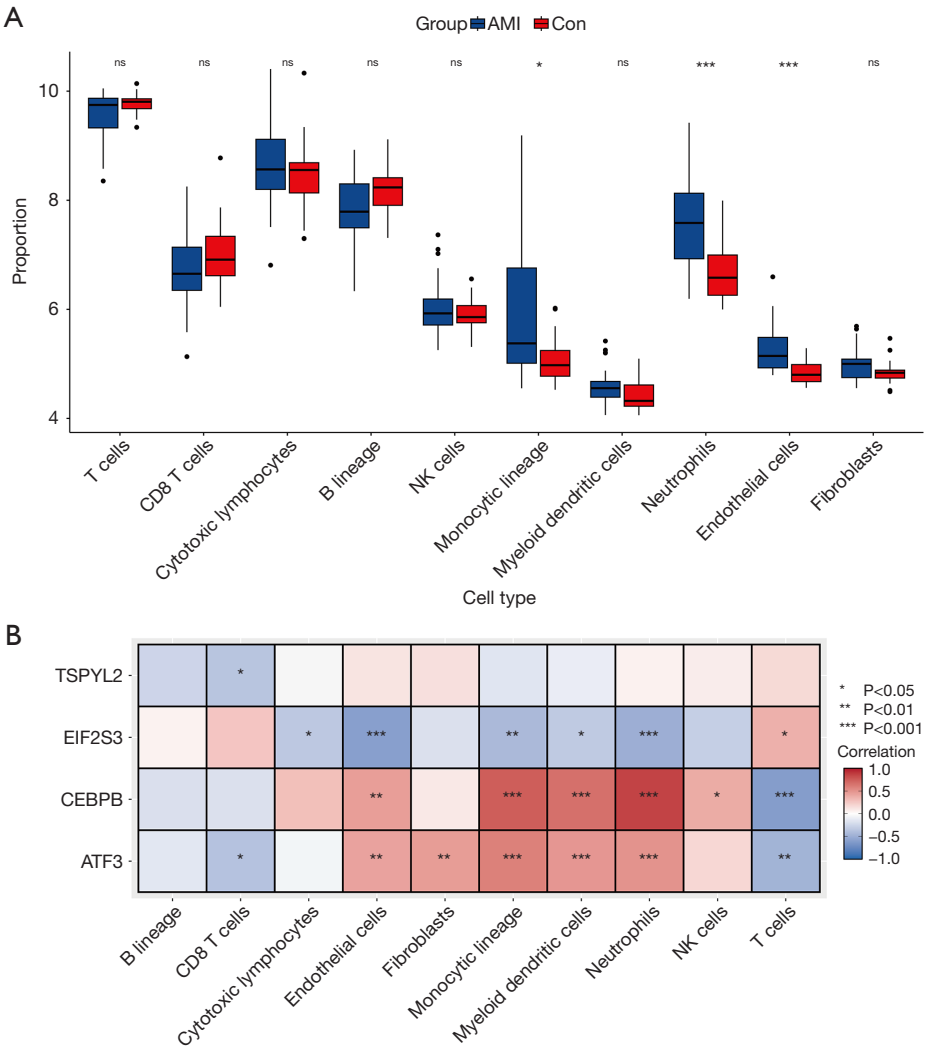

Figure 7 Immune landscape analysis by MCPcounter algorithm. (A) Using the MCPcounter algorithm to explore the differences in the immune microenvironment between AMI patients and normal controls. (B) Using the MCPcounter algorithm to analysis immune cell infiltration of model genes. *, P<0.05; **, P<0.01; ***, P<0.001. ns, not significant; AMI, acute myocardial infarction; Con, control; NK, natural killer.

Classifying AMI patients through consensus clustering

Based on the unsupervised clustering results, the AMI patients were classified into two distinct clusters (*Figure 8A*,*8B*). The overall expression profiles of the UPR-DEGs differed between the two clusters (*Figure 8C*). We observed that *CXCL8* exhibited the highest expression in cluster 1, and *EIF2S3* exhibited the highest expression in cluster 2. These two genes may be characteristic genes for each cluster. We further assessed the UPR pathway gene enrichment scores of each sample using the ssGSEA algorithm, and the results showed that the activation of the UPR pathway in cluster 1 was greater than that in cluster 2 (*Figure 8D*). In addition, the infiltration of immune cells and the secretion of inflammatory markers were significantly different between the two clusters (*Figure 8E*,*8F*). The proportion of T cells was greater in cluster 2 than in cluster 1, but the proportions of monocytic lineage cells, myeloid dendritic cells, and neutrophils were greater in cluster 1. In terms of inflammatory markers, *TP53* was highly expressed in cluster 2; however, the other DEGs were highly expressed in cluster 1. In summary, we found that the activation of UPR pathway genes, inflammatory

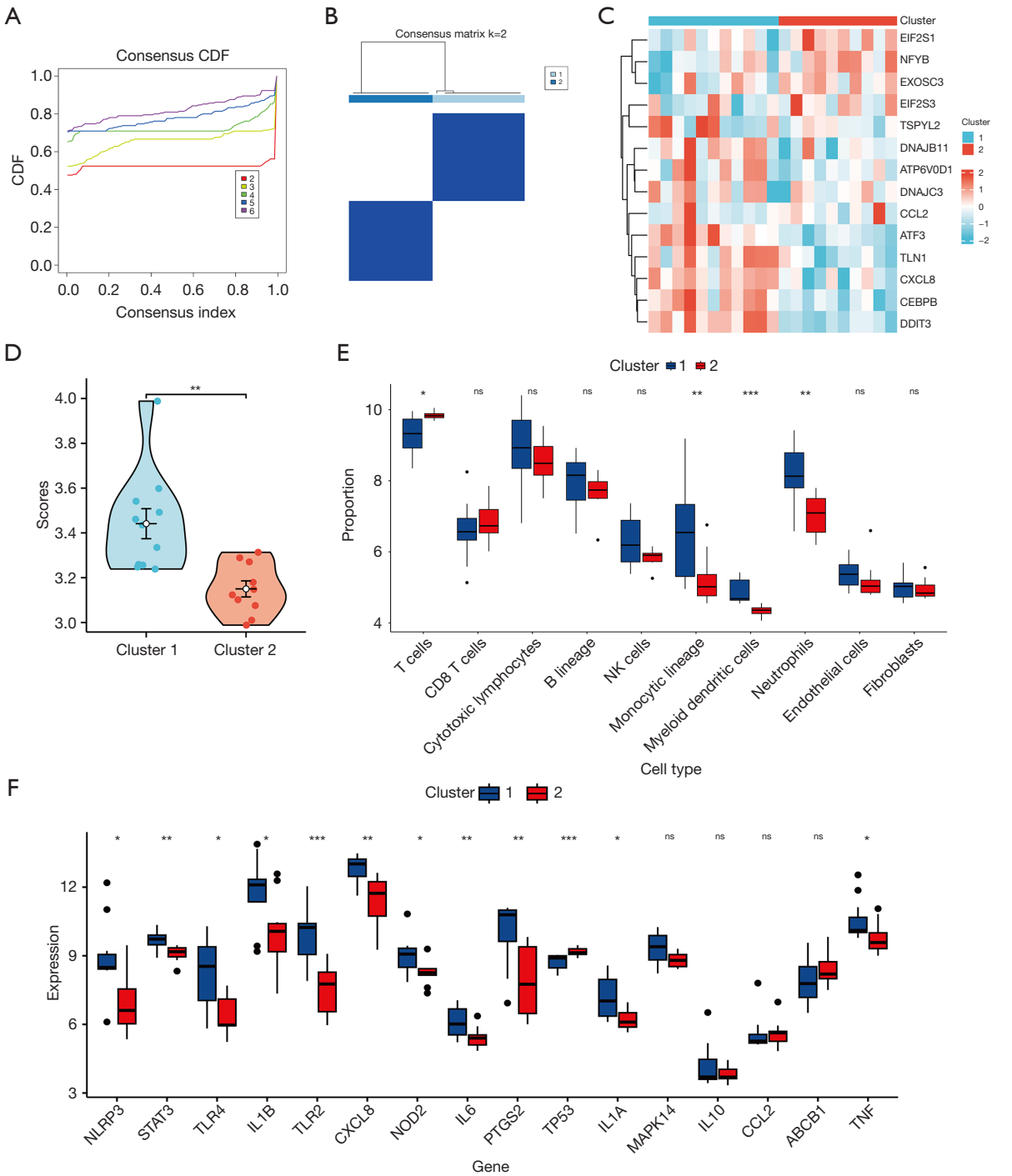

Figure 8 Consensus clustering analysis. (A) The CDF distribution diagram of consistency clustering analysis. (B) Consensus matrix heatmap. (C) Heatmap visualizing the expression of UPR-related genes in the two clusters. (D) Violin plots show the difference of ssGSEA scores between the two clusters. (E) Immune cell Infiltration in different clusters. (F) The expression of inflammatory factor in different clusters. *, P<0.05; **, P<0.01; ***, P<0.001. ns, not significant; CDF, cumulative distribution function; UPR, unfolded protein response; ssGSEA, single sample gene set enrichment analysis; NK, natural killer.

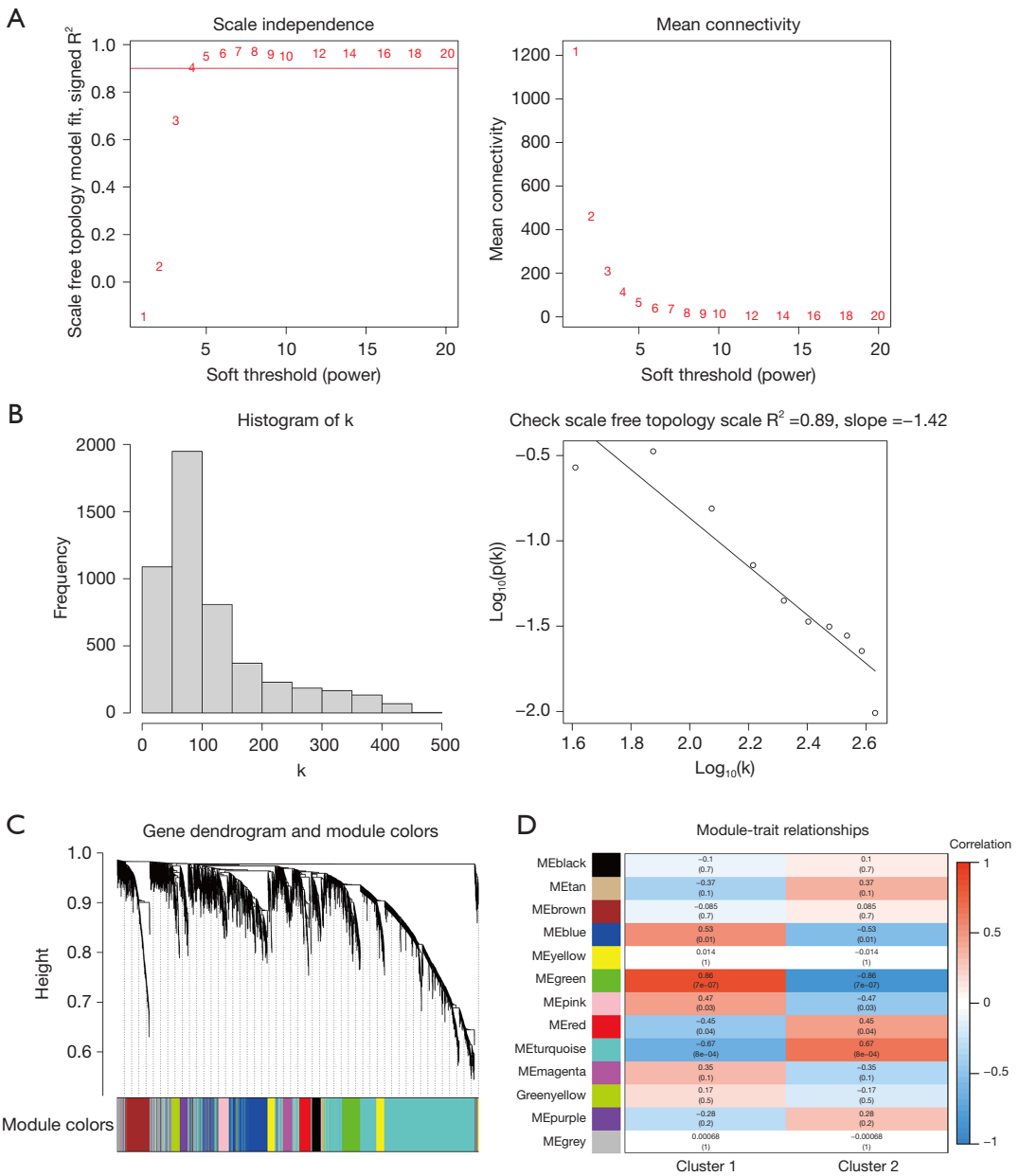

Figure 9 Construction of WGCNA modules. (A) Analysis of the scale-free index and the mean connectivity for different soft thresholds. (B) Histogram of connectivity distribution and checking the scale-free topology when β=4. (C) Cluster dendrogram. (D) Heatmap of the module-trait relationships. WGCNA, weighted gene coexpression network analysis.

markers and immune cells in cluster 1 was greater than that in cluster 2.

Functional enrichment analysis of different clusters

We used WGCNA to identify coexpressed gene modules in different clusters. First, we constructed a sample clustering tree and clustering samples for the processing of outliers.

Then, the soft threshold based on the scale-free topology fitting index R^2 was selected (R^2=0.89; soft thresholding power β=4; slope =−1.42) (*Figure 9A,9B*). Subsequently, we used a one-step method to construct a coexpression matrix, and a total of 13 gene modules were obtained through dynamic hybrid shearing (*Figure 9C*). Later, the correlations

Table 1 GO enrichment analysis in different gene modules

Module	GO ID	Term name	P value	FDR	Size
Black	GO:0006364	rRNA processing	1.10E−07	0.00017	174
Black	GO:0016072	rRNA metabolic process	6.30E−07	0.00076	174
Blue	GO:0005759	Mitochondrial matrix	5.30E−05	0.031	713
Blue	GO:0034660	ncRNA metabolic process	6.60E−05	0.036	713
Brown	GO:0048646	Anatomical structure formation involved in morphogenesis	8.30E−17	9.90E−13	344
Brown	GO:0062023	Collagen-containing extracellular matrix	2.10E−15	2.10E−11	344
Green	GO:0042101	T cell receptor complex	2.70E−06	0.0026	250
Greenyellow	GO:0007059	Chromosome segregation	2.30E−24	1.50E−19	115
Greenyellow	GO:0098813	Nuclear chromosome segregation	3.20E−23	1.50E−18	115
Magenta	GO:0030326	Embryonic limb morphogenesis	2.70E−05	0.018	152
Magenta	GO:0035113	Embryonic appendage morphogenesis	2.70E−05	0.018	152
Pink	GO:0006281	DNA repair	3.50E−06	0.0033	154
Pink	GO:0006974	Cellular response to DNA damage stimulus	4.40E−05	0.027	154
Purple	GO:0050853	B cell receptor signaling pathway	4.90E−12	2.40E−08	116
Purple	GO:0042113	B cell activation	3.30E−10	1.10E−06	116
Red	GO:0030527	Structural constituent of chromatin	4.90E−32	1.30E−26	178
Red	GO:0000786	Nucleosome	5.20E−29	7.20E−24	178
Tan	GO:0006139	Nucleobase-containing compound metabolic process	2.60E−05	0.017	52
Tan	GO:0090304	Nucleic acid metabolic process	3.30E−05	0.021	52
Turquoise	GO:0031410	Cytoplasmic vesicle	4.00E−20	1.00E−15	2,099
Turquoise	GO:0097708	Intracellular vesicle	5.80E−20	1.30E−15	2,099

rRNA, ribosomal RNA; ncRNA, non-coding RNA; GO, Gene Ontology; FDR, false discovery rate.

of gene modules with different clusters were presented via heatmaps, and we observed that the MEgreen module, MEturquoise module and MEblue module were correlated with different clusters, with correlation coefficients of 0.86, 0.67 and 0.53, respectively (*Figure 9D*). Furthermore, we used the R package "anRichment" to perform GO enrichment analysis of different gene modules. We found that the genes within the MEgreen module were primarily involved in processes involving the T-cell receptor complex. The MEturquoise module was found to be enriched in processes such as cytoplasmic vesicles, intracellular vesicles, and secretory vesicles. The MEblue module was predominantly linked to the mitochondrial matrix, non-coding RNA (ncRNA) metabolic processes, and transfer RNA (tRNA) metabolic processes (*Table 1*).

Discussion

Mitochondria play essential roles in various physiological processes, such as energy production, the immune response and apoptosis (19). Due to the diversity of mitochondrial functions, maintaining mitochondrial homeostasis is critical for cell survival and heart function. Mitochondrial homeostasis is regulated by quality control mechanisms, including mitochondrial dynamics, mitophagy, biogenesis and the UPR, and the associated molecular machinery is highly interconnected (1,20). In response to stress, such as oxidative stress, metabolic dysfunction or mitochondrial DNA impairment, the UPR is activated and maintains protein quality and mitochondrial function by promoting the expression of mitochondrial chaperones (HSP10,

HSP60, and DNAJ) and proteases (CLPP and LONP1) (1,21,22). Mitochondrial chaperones mainly promote the correct folding of newly imported proteins, and proteases mainly degrade misfolded or damaged proteins within mitochondria (22,23). However, when stress exceeds a certain threshold, the UPR cannot repair dysfunctional mitochondria. This triggers mitochondrial fission to separate the damaged region from the healthy mitochondrial network, and this region is cleared by mitophagy (1,9). Although UPR activation provides a cytoprotective advantage, prolonging UPR activation is detrimental and can lead to cell death (24,25). Mitochondrial UPR has been widely studied in the field of cancer. It serves as an important support system in cancer to maintain mitochondrial health, and promote tumor growth and proliferation (26). It has been reported that components of mitochondrial UPR such as HSP10, HSP60, CLPP and LONP1, are overexpressed in various cancers (26). Additionally, mitochondrial UPR upregulates the expression of growth differentiation factor 15 (GDF-15) in tumor, thus promoting the invasion and migration of cancer cells (27). Targeting the UPR pathway may be a potentially effective treatment for various cancers. However, the activation of the UPR adaptive pathways may lead to drug resistance (28). Mitochondrial UPR has also been studied in different cardiac disease models, and its activation in mammals is mediated by the transcription factors CHOP (C/EBP homologous protein), ATF4, and ATF5 (1). A study revealed that pharmacologic UPR activation reduces MI size and improves ventricular function after cardiac reperfusion injury in wild-type mice but not in ATF5-deficient mice (29). Moreover, ATF5 is a downstream effector of PGC-1α. The PGC-1α/ATF5 axis activates mitochondrial UPR, which mediates the cardioprotective role under pathological cardiac hypertrophy (30). In addition, MRPS5/ATF4 signaling has been shown to play an important role in cardiomyocyte proliferation, cardiac function and heart regeneration by regulating cell division-associated gene transcription after cardiac injury (31). Conversely, there is evidence that UPR may be associated with harmful events in the heart. Elevated LONP1 activity is a mediator of hypoxia-induced cardiomyocyte apoptosis, while loss of CLPP increases the expression of respiratory chain subunits and alleviates cardiomyopathy (32,33). Therefore, differential regulation of individual components of the UPR to alleviate stress responses may provide a promising avenue for therapeutic intervention in MI.

Our research identified four key genes associated with the UPR pathway that were involved in the occurrence of MI, namely, *CEBPB*, *ATF3*, *TSPYL2* and *EIF2S3*. The AUC values of these 4 genes were all greater than 0.7. In addition, the diagnostic model constructed from these 4 genes showed excellent performance, with an AUC value of 0.94, suggesting that these genes have high accuracy and specificity in distinguishing AMI patients from normal control individuals. Among these genes, *CEBPB* is a member of the bZIP family of transcription factors and can promote UPR activation through cooperation with the CHOP (34,35). Under mitochondrial stress, *CEBPB* is upregulated and forms a dimer with CHOP, which increases the expression levels of mitochondrial chaperones and proteases (34,36). *CEBPB* is involved in a variety of BPs, such as regulating cell proliferation and differentiation, inflammation, and the expression of immune genes (37,38). In addition, *CEBPB* accelerates the atherosclerotic process by increasing the release of oxidized low-density lipoprotein, which mediates the secretion of inflammatory factors from foam cells (39). In a mouse model of atherosclerosis, the expression of *CEBPB* was significantly greater in the atherosclerosis group than in the control group, and the expression level increased with the aggravation of atherosclerotic lesions (39). In addition, it has been reported that the induction of *CEBPB* leads to metabolic deregulation, excess lipid accumulation and endoplasmic reticulum stress in a rat model of cardiac hypertrophy, and the knockdown of *CEBPB* could prevent impaired cardiac function (40). Moreover, a previous study using integrated bioinformatics and machine learning algorithms reported that *CEBPB* plays a critical role in the development of ischaemic cardiomyopathy (41). These findings are consistent with our findings, as our study revealed that *CEBPB* is highly expressed in the AMI group, which may lead to UPR overactivation. However, the specific mechanisms underlying these effects need further study. *ATF3* is a crucial transcription factor and a member of the ATF/cyclic adenosine monophosphate (cAMP) response element binding family (42). A previous study reported that *ATF3* plays an indispensable role in the PERK/eIF2 signalling pathway of the UPR and that the UPR enhances *ATF3* expression via p-eIF2-ATF4 signalling (43). *ATF3* is weakly expressed in various cells and can be induced in stressed tissues, such as atherosclerotic plaques and ischaemic heart tissue (44). *ATF3* controls the expression of chemokines and cytokines to inhibit inflammatory responses, which is beneficial for stressed tissues (45). It has been reported that the cardioprotective

effects of ischaemic preconditioning are due to the activation of adaptive UPR signalling, including *ATF3*, and the deletion of *ATF3* abolishes the cardioprotective effects of ischaemic preconditioning (46). Our study revealed that *ATF3* is highly expressed in the AMI group, which may be a protective mechanism of the body against this disease. In addition, the level of *ATF3* is thought to be related to atherosclerotic plaque stability, and the expression of *ATF3* in macrophages present in ruptured atherosclerotic plaques is lower than that in stable atherosclerotic plaques (47). Thus, *ATF3* plays a role in both atherosclerosis and the UPR and may be a new prognostic biomarker and therapeutic target for AMI. *EIF2S3* encodes a subunit of the eIF2 complex, which is an important translation initiation factor that promotes protein synthesis initiation by binding with Met-tRNA (48). *TSPYL2* is an X-linked gene encoding a nucleosome assembly protein that plays important roles in regulating cell growth and the DNA damage response (49). A previous study revealed that the expression of *TSPYL2* is increased in the aortas of diabetic $Apoe^{-/-}$ mice and that this increase is accompanied by the progressive development of atherosclerosis and increased atherosclerotic plaque area. Knockdown of *TSPYL2* can block the profibrotic effect of TGF-β, thus preventing atherosclerosis (50). Thus, *TSPYL2* appears to be an attractive molecular target for treating atherosclerosis.

The immune cells found in the heart include neutrophils, dendritic cells, monocytes, T cells, B cells, eosinophils, mast cells, and macrophages (51). All of these cell types play important roles in maintaining cardiac function. Ischaemia induces significant alterations in the immune cell landscape in the heart. Our analysis revealed that activated memory CD4 T cells, resting NK cells, monocytes, activated dendritic cells, activated mast cells and neutrophils were highly abundant in the AMI group, and resting memory CD4 T cells and gamma delta T cells were less abundant than those in the control group. Immune activation is often associated with the reprogramming of cellular metabolism. Immune cells sense environmental and metabolic demands, and induce specialized stress responses within the cell, mitochondria serve as the central hub of metabolic signaling in cells. It has been reported that during stress, mitochondrial UPR promotes rewiring of cellular metabolism, such as increased glycolysis, to relieve mitochondrial stress and alter cellular metabolism to promote survival (7). Enhanced glycolysis enables immune cells to produce sufficient adenosine triphosphate (ATP) and biosynthetic intermediates to carry out their particular effector functions. For macrophages, this includes phagocytosis and inflammatory cytokine production, for dendritic cells, this includes antigen presentation, and for T cells this includes the production of effector cytokines. In addition, enhanced glycolysis also occurs in activated NK cells and activated B cells (52). Necrotic cardiomyocytes following infarction release danger signals that activate immune pathways and trigger an inflammatory response (53). This promotes adhesive interactions between leukocytes and endothelial cells, leading to the extravasation of neutrophils and monocytes (53). Subsequently, monocytes differentiate into macrophages to mediate the development and resolution of inflammation, together with neutrophils (53). Mast cells are abundant in coronary lesions and participate in plaque rupture (54). Treatment with ketotifen (a mast cell membrane stabilizer) reportedly reduces ischaemia/reperfusion injury in isolated rat hearts (55). Dendritic cells may alter the post-MI healing process by activating T lymphocytes, secreting inflammatory cytokines and activating fibroblasts (56). A previous study reported that the depletion of conventional dendritic cells in chimeric mice is related to a reduction in infarct size and an improvement in cardiac function after MI (56). In addition, $CD4^+$ T cells are thought to be closely related to injury size, and RAG1 knockout (KO) mice lacking T lymphocytes have smaller MI sizes than control mice (57). Among the UPR pathway-related genes, *CEBPB* was positively correlated with neutrophils. *CEBPB* is reported to be crucial for 'emergency' granulopoiesis (58). *CEBPB* can promote the differentiation and migration of neutrophils and participate in the expression and production of inflammatory cytokines in neutrophils (59). A previous study reported that in neutrophils from *CEBPB* knockout mice, the levels of IL-6, IL-10, and IL-12 were markedly decreased compared to those in neutrophils from wild-type mice (60). *CEBPB* has been shown to form complexes with transcription factors such as PU.1 to regulate the expression of genes involved in neutrophil differentiation and function (61). *ATF3* has been shown to enhance neutrophil chemotaxis by promoting TIAM2 expression (62). Our study revealed that *ATF3* was positively correlated with neutrophils. However, whether this correlation is related to TIAM2 remains to be verified. In addition, several drugs or compounds have been reported to exert powerful protective effects against cardiovascular disease by regulating these biomarkers. Alpha-lipoic acid, a naturally occurring compound, has been shown to improve the progression of cardiac hypertrophy via inhibiting *CEBPB*

activation (63). Atorvastatin, not only reduces blood lipids but also protects hypertrophic cardiomyocytes induced by angiotensin II by downregulating *CEBPB* expression (64). Moreover, Panax notoginseng saponins have been reported to improve cardiac function and fibrosis in MI rats via regulating ATF3/MAP2K3/p38 MAPK signaling pathways (65). However, the effects of these drugs or compounds on the mitochondrial UPR in the post-infarcted heart are still unknown, and the mitochondrial UPR may be a new target for the treatment of AMI.

A previous study reported that AMI can be further subclassified by a suspected pathophysiology (66). Type 1 MI is caused by atherothrombotic coronary artery disease and is usually initiated by atherothrombotic plaque rupture (66). Type 2 MI is caused by an acute imbalance in oxygen supply and demand without atherothrombosis (66). Furthermore, we analysed the expression profiles of genes related to the UPR pathway, immune cell infiltration, and inflammatory cytokine secretion in patients with AMI. Our results indicate that there are some differences in these characteristics among AMI patients in different clusters. Compared with those in cluster 2, the numbers of monocytes and neutrophils, which play important roles in atherosclerosis, were significantly greater in cluster 1, and the levels of UPR pathway-related genes and inflammatory factors were increased. Therefore, we speculate that UPR-related genes play important roles in the occurrence and development of atherosclerosis. However, due to the lack of clinical information on patient samples, the regulatory mechanism of AMI subtypes requires further study.

There are some limitations in this study that should be acknowledged. First, our study selected only UPR-related genes from the PathCards database. Thus, the identification of more UPR-related genes is needed. Second, our results were derived from relatively small sample sizes, which may cause deviations in the experimental results. However, we carried out internal and external validations to compensate for this limitation. Third, this is a bioinformatics study that is based on secondary mining and analysis of previous data and has not been experimentally verified. Further investigations based on animal experiments and clinical studies are needed.

Conclusions

In the present study, we analysed the microarray data of AMI patients and revealed that the relationships among the expression of genes related to the UPR pathway, immune cell infiltration, and inflammatory factor secretion were closed in patients with AMI. *CEBPB*, *ATF3*, *EIF2S3*, and *TSPYL2* were identified as novel diagnostic biomarkers for AMI. Moreover, a diagnostic model based on these genes that has high applicability value for identifying AMI patients was constructed. Finally, we constructed a nomogram with these four biomarkers to predict the risk for estimating the status of patients with AMI. Our study provides new insights into the underlying mechanisms of AMI and lays a foundation for therapeutic strategies for AMI patients.

Acknowledgments

Funding: None.

Footnote

Reporting Checklist: The authors have completed the TRIPOD reporting checklist. Available at https://jtd.amegroups.com/article/view/10.21037/jtd-24-622/rc

Peer Review File: Available at https://jtd.amegroups.com/article/view/10.21037/jtd-24-622/prf

Conflicts of Interest: All authors have completed the ICMJE uniform disclosure form (available at https://jtd.amegroups.com/article/view/10.21037/jtd-24-622/coif). The authors have no conflicts of interest to declare.

Ethical Statement: The authors are accountable for all aspects of the work in ensuring that questions related to the accuracy or integrity of any part of the work are appropriately investigated and resolved. The study was conducted in accordance with the Declaration of Helsinki (as revised in 2013).

References

1. Bai Y, Wu J, Yang Z, et al. Mitochondrial quality control in cardiac ischemia/reperfusion injury: new insights into mechanisms and implications. Cell Biol Toxicol 2023;39:33-51.
2. Fazel R, Joseph TI, Sankardas MA, et al. Comparison of Reperfusion Strategies for ST-Segment-Elevation Myocardial Infarction: A Multivariate Network Meta-analysis. J Am Heart Assoc 2020;9:e015186.
3. Kural MH, Wang J, Gui L, et al. Fas ligand and nitric oxide combination to control smooth muscle growth while sparing endothelium. Biomaterials 2019;212:28-38.
4. Lieder HR, Kleinbongard P, Skyschally A, et al. Vago-Splenic Axis in Signal Transduction of Remote Ischemic Preconditioning in Pigs and Rats. Circ Res 2018;123:1152-63.
5. Zhu MX, Sun SQ, Fan GB, et al. Knowledge mapping of research on the mitochondrial unfolded protein response: a bibliometric and visual analysis. Ann Transl Med 2023;11:64.
6. Pellegrino MW, Nargund AM, Haynes CM. Signaling the mitochondrial unfolded protein response. Biochim Biophys Acta 2013;1833:410-6.
7. Zhu L, Luo X, Fu N, et al. Mitochondrial unfolded protein response: A novel pathway in metabolism and immunity. Pharmacol Res 2021;168:105603.
8. Yao Y, Zhao J, Zhou X, et al. Potential role of a three-gene signature in predicting diagnosis in patients with myocardial infarction. Bioengineered 2021;12:2734-49.
9. Yu H, Ji X, Ouyang Y. Unfolded protein response pathways in stroke patients: a comprehensive landscape assessed through machine learning algorithms and experimental verification. J Transl Med 2023;21:759.
10. Ritchie ME, Phipson B, Wu D, et al. limma powers differential expression analyses for RNA-sequencing and microarray studies. Nucleic Acids Res 2015;43:e47.
11. Yu G, Wang LG, Han Y, et al. clusterProfiler: an R package for comparing biological themes among gene clusters. OMICS 2012;16:284-7.
12. Hirata T, Arai Y, Yuasa S, et al. Associations of cardiovascular biomarkers and plasma albumin with exceptional survival to the highest ages. Nat Commun 2020;11:3820.
13. Méric G, Mageiros L, Pensar J, et al. Disease-associated genotypes of the commensal skin bacterium Staphylococcus epidermidis. Nat Commun 2018;9:5034.
14. Linden A. Measuring diagnostic and predictive accuracy in disease management: an introduction to receiver operating characteristic (ROC) analysis. J Eval Clin Pract 2006;12:132-9.
15. Chen B, Khodadoust MS, Liu CL, et al. Profiling Tumor Infiltrating Immune Cells with CIBERSORT. Methods Mol Biol 2018;1711:243-59.
16. Becht E, Giraldo NA, Lacroix L, et al. Estimating the population abundance of tissue-infiltrating immune and stromal cell populations using gene expression. Genome Biol 2016;17:218.
17. Wilkerson MD, Hayes DN. ConsensusClusterPlus: a class discovery tool with confidence assessments and item tracking. Bioinformatics 2010;26:1572-3.
18. Langfelder P, Horvath S. WGCNA: an R package for weighted correlation network analysis. BMC Bioinformatics 2008;9:559.
19. Spinelli JB, Haigis MC. The multifaceted contributions of mitochondria to cellular metabolism. Nat Cell Biol 2018;20:745-54.
20. Bai Y, Yang Y, Gao Y, et al. Melatonin postconditioning ameliorates anoxia/reoxygenation injury by regulating mitophagy and mitochondrial dynamics in a SIRT3-dependent manner. Eur J Pharmacol 2021;904:174157.
21. Song J, Herrmann JM, Becker T. Quality control of the mitochondrial proteome. Nat Rev Mol Cell Biol 2021;22:54-70.
22. Smyrnias I. The mitochondrial unfolded protein response and its diverse roles in cellular stress. Int J Biochem Cell Biol 2021;133:105934.
23. Münch C, Harper JW. Mitochondrial unfolded protein response controls matrix pre-RNA processing and translation. Nature 2016;534:710-3.
24. Hetz C, Zhang K, Kaufman RJ. Mechanisms, regulation and functions of the unfolded protein response. Nat Rev Mol Cell Biol 2020;21:421-38.
25. Wang S, Wang Z, Fan Q, et al. Ginkgolide K protects the heart against endoplasmic reticulum stress injury by activating the inositol-requiring enzyme 1α/X box-binding protein-1 pathway. Br J Pharmacol 2016;173:2402-18.
26. Inigo JR, Chandra D. The mitochondrial unfolded protein response (UPR(mt)): shielding against toxicity to mitochondria in cancer. J Hematol Oncol 2022;15:98.
27. Kang YE, Kim JM, Lim MA, et al. Growth Differentiation Factor 15 is a Cancer Cell-Induced Mitokine That Primes Thyroid Cancer Cells for Invasiveness. Thyroid 2021;31:772-86.
28. Zheng S, Wang X, Liu H, et al. iASPP suppression mediates terminal UPR and improves BRAF-inhibitor

sensitivity of colon cancers. Cell Death Differ 2023;30:327-40.
29. Wang YT, Lim Y, McCall MN, et al. Cardioprotection by the mitochondrial unfolded protein response requires ATF5. Am J Physiol Heart Circ Physiol 2019;317:H472-8.
30. Zhang B, Tan Y, Zhang Z, et al. Novel PGC-1α/ATF5 Axis Partly Activates UPR(mt) and Mediates Cardioprotective Role of Tetrahydrocurcumin in Pathological Cardiac Hypertrophy. Oxid Med Cell Longev 2020;2020:9187065.
31. Gao F, Liang T, Lu YW, et al. Reduced Mitochondrial Protein Translation Promotes Cardiomyocyte Proliferation and Heart Regeneration. Circulation 2023;148:1887-906.
32. Kuo CY, Chiu YC, Lee AY, et al. Mitochondrial Lon protease controls ROS-dependent apoptosis in cardiomyocyte under hypoxia. Mitochondrion 2015;23:7-16.
33. Seiferling D, Szczepanowska K, Becker C, et al. Loss of CLPP alleviates mitochondrial cardiomyopathy without affecting the mammalian UPRmt. EMBO Rep 2016;17:953-64.
34. Zhao Q, Wang J, Levichkin IV, et al. A mitochondrial specific stress response in mammalian cells. EMBO J 2002;21:4411-9.
35. Martin LJ, Nguyen HT. Basic Leucine Zipper Transcription Factors as Important Regulators of Leydig Cells' Functions. Int J Mol Sci 2022;23:12887.
36. Zhou Z, Fan Y, Zong R, et al. The mitochondrial unfolded protein response: A multitasking giant in the fight against human diseases. Ageing Res Rev 2022;81:101702.
37. Chen JJ, Huang WC, Chen CC. Transcriptional regulation of cyclooxygenase-2 in response to proteasome inhibitors involves reactive oxygen species-mediated signaling pathway and recruitment of CCAAT/enhancer-binding protein delta and CREB-binding protein. Mol Biol Cell 2005;16:5579-91.
38. Guo L, Huang JX, Liu Y, et al. Transactivation of Atg4b by C/EBPβ promotes autophagy to facilitate adipogenesis. Mol Cell Biol 2013;33:3180-90.
39. Rahman SM, Baquero KC, Choudhury M, et al. C/EBPβ in bone marrow is essential for diet induced inflammation, cholesterol balance, and atherosclerosis. Atherosclerosis 2016;250:172-9.
40. Banerjee D, Datta Chaudhuri R, Niyogi S, et al. Metabolic impairment in response to early induction of C/EBPβ leads to compromised cardiac function during pathological hypertrophy. J Mol Cell Cardiol 2020;139:148-63.
41. Guo L, Xu CE. Integrated bioinformatics and machine learning algorithms reveal the critical cellular senescence-associated genes and immune infiltration in heart failure due to ischemic cardiomyopathy. Front Immunol 2023;14:1150304.
42. Ku HC, Cheng CF. Master Regulator Activating Transcription Factor 3 (ATF3) in Metabolic Homeostasis and Cancer. Front Endocrinol (Lausanne) 2020;11:556.
43. Liu Z, Shi Q, Song X, et al. Activating Transcription Factor 4 (ATF4)-ATF3-C/EBP Homologous Protein (CHOP) Cascade Shows an Essential Role in the ER Stress-Induced Sensitization of Tetrachlorobenzoquinone-Challenged PC12 Cells to ROS-Mediated Apoptosis via Death Receptor 5 (DR5) Signaling. Chem Res Toxicol 2016;29:1510-8.
44. Hai T, Wolford CC, Chang YS. ATF3, a hub of the cellular adaptive-response network, in the pathogenesis of diseases: is modulation of inflammation a unifying component? Gene Expr 2010;15:1-11.
45. Nguyen CT, Kim EH, Luong TT, et al. TLR4 mediates pneumolysin-induced ATF3 expression through the JNK/p38 pathway in Streptococcus pneumoniae-infected RAW 264.7 cells. Mol Cells 2015;38:58-64.
46. Brooks AC, Guo Y, Singh M, et al. Endoplasmic reticulum stress-dependent activation of ATF3 mediates the late phase of ischemic preconditioning. J Mol Cell Cardiol 2014;76:138-47.
47. Qin W, Yang H, Liu G, et al. Activating transcription factor 3 is a potential target and a new biomarker for the prognosis of atherosclerosis. Hum Cell 2021;34:49-59.
48. Gregory LC, Ferreira CB, Young-Baird SK, et al. Impaired EIF2S3 function associated with a novel phenotype of X-linked hypopituitarism with glucose dysregulation. EBioMedicine 2019;42:470-80.
49. Magni M, Buscemi G, Maita L, et al. TSPYL2 is a novel regulator of SIRT1 and p300 activity in response to DNA damage. Cell Death Differ 2019;26:918-31.
50. Pham Y, Tu Y, Wu T, et al. Cell division autoantigen 1 plays a profibrotic role by modulating downstream signalling of TGF-beta in a murine diabetic model of atherosclerosis. Diabetologia 2010;53:170-9.
51. Swirski FK, Nahrendorf M. Cardioimmunology: the immune system in cardiac homeostasis and disease. Nat Rev Immunol 2018;18:733-44.
52. O'Neill LA, Kishton RJ, Rathmell J. A guide to immunometabolism for immunologists. Nat Rev Immunol 2016;16:553-65.
53. Prabhu SD, Frangogiannis NG. The Biological Basis for Cardiac Repair After Myocardial Infarction: From Inflammation to Fibrosis. Circ Res 2016;119:91-112.

54. Kologrivova I, Shtatolkina M, Suslova T, et al. Cells of the Immune System in Cardiac Remodeling: Main Players in Resolution of Inflammation and Repair After Myocardial Infarction. Front Immunol 2021;12:664457.
55. Jaggi AS, Singh M, Sharma A, et al. Cardioprotective effects of mast cell modulators in ischemia-reperfusion-induced injury in rats. Methods Find Exp Clin Pharmacol 2007;29:593-600.
56. Lee JS, Jeong SJ, Kim S, et al. Conventional Dendritic Cells Impair Recovery after Myocardial Infarction. J Immunol 2018;201:1784-98.
57. Yang Z, Day YJ, Toufektsian MC, et al. Myocardial infarct-sparing effect of adenosine A2A receptor activation is due to its action on CD4+ T lymphocytes. Circulation 2006;114:2056-64.
58. Thind MK, Uhlig HH, Glogauer M, et al. A metabolic perspective of the neutrophil life cycle: new avenues in immunometabolism. Front Immunol 2023;14:1334205.
59. Cloutier A, Guindi C, Larivée P, et al. Inflammatory cytokine production by human neutrophils involves C/EBP transcription factors. J Immunol 2009;182:563-71.
60. Akagi T, Saitoh T, O'Kelly J, et al. Impaired response to GM-CSF and G-CSF, and enhanced apoptosis in C/EBPbeta-deficient hematopoietic cells. Blood 2008;111:2999-3004.
61. Chen L, Ge B, Casale FP, et al. Genetic Drivers of Epigenetic and Transcriptional Variation in Human Immune Cells. Cell 2016;167:1398-1414.e24.
62. Boespflug ND, Kumar S, McAlees JW, et al. ATF3 is a novel regulator of mouse neutrophil migration. Blood 2014;123:2084-93.
63. Zou J, Gan X, Zhou H, et al. Alpha-lipoic acid attenuates cardiac hypertrophy via inhibition of C/EBPβ activation. Mol Cell Endocrinol 2015;399:321-9.
64. Chen Y, Yu S, Zhang N, et al. Atorvastatin prevents Angiotensin II induced myocardial hypertrophy in vitro via CCAAT/enhancer-binding protein β. Biochem Biophys Res Commun 2017;486:423-30.
65. Ma RF, Chen G, Li HZ, et al. Panax Notoginseng Saponins Inhibits Ventricular Remodeling after Myocardial Infarction in Rats Through Regulating ATF3/MAP2K3/p38 MAPK and NF κ B Pathway. Chin J Integr Med 2020;26:897-904.
66. DeFilippis AP, Chapman AR, Mills NL, et al. Assessment and Treatment of Patients With Type 2 Myocardial Infarction and Acute Nonischemic Myocardial Injury. Circulation 2019;140:1661-78.

Cite this article as: Bai Y, Niu Z, Yang Z, Sun Y, Yan W, Wu A, Wei C. Integrated bioinformatics and machine learning algorithms reveal the unfolded protein response pathways and immune infiltration in acute myocardial infarction. J Thorac Dis 2024;16(10):6496-6515. doi: 10.21037/jtd-24-622